Observation of oxygen pyramid tilting induced polarization rotation in strained $BiFeO_3$ thin film

Dongsheng Song[a,b], Heng-Jui Liu[c], András Kovács[b], Rafal E. Dunin-Borkowski[b], Ying-Hao Chu[d], Jing Zhu[a,*]

[a]National Center for Electron Microscopy in Beijing, Key Laboratory of Advanced Materials (MOE) and The State Key Laboratory of New Ceramics and Fine Processing, School of Materials Science and Engineering, Tsinghua University, Beijing 100084, China.

[b]Ernst Ruska-Centre for Microscopy and Spectroscopy with Electrons and Peter Grünberg Institute, Forschungszentrum Jülich, D-52425 Jülich, Germany.

[c]Department of Materials Science and Engineering, National Chung Hsing University, Taichung 40227, Taiwan.

[d]Department of Materials Science and Engineering, National Chiao Tung University, Hsinchu 30010, Taiwan.

*Corresponding author: jzhu@mail.tsinghua.edu.cn

Abstract

Oxygen octahedral tilting has been recognized to strongly interact with spin, charge, orbital and lattice degrees of freedom in perovskite oxides. Here, we observe a strain-driven stripe-like morphology of two supertetragonal (monoclinic Cc and Cm) phases in the strained $BiFeO_3/LaAlO_3$ thin films. The two supertetragonal phases have a similar giant axial ratio but differences in oxygen pyramid tilting mode. Especially, the competition between polar instability and oxygen pyramid tilting is identified using atomically resolved scanning transmission electron microscopy, leading to the polarization rotation across the phase boundary. In addition, microtwins are observed in the Cc phase. Our findings provide new insights of the coupling between ferroelectric polarization and oxygen pyramid tilting in oxide thin films and will help to design novel phase morphology with desirable ferroelectric polarization and properties for new applications in perovskite oxides.

1.! Introduction

The oxygen octahedral tilting, which is usually defined as the configuration of the corner-connective -BO_6- octahedra in perovskite oxides (ABO_3), has been recognized to strongly interact with these degrees of freedom (spin, charge, orbital and lattice)[1–3] and affect the macroscopic electrical/magnetic properties[4–14]. Among them, the interplay between ferroelectric polar order and octahedra tilting has been theoretically[4] and experimentally[5, 13] studied in the ABO_3 thin films, such as the ferroelectricity at the interface between nonpolar ABO_3 oxides[4, 15, 16], polarization rotation in $PbTiO_3$ thin films[13], suppression of polarization in the $BiFeO_3$ (BFO) thin films[5]. Moreover, the manipulation of polarization by oxygen octahedra tilting could further affect their ferroelectric or piezoelectric response to external electrical field, demonstrating an extraordinary opportunity to control the multifunctional properties in ABO_3 oxides.

Different oxygen octahedral titling modes will modify the polarization in different ways[5, 13]. The ABO_3 oxides thin films are always exhibited with plenty of phase structures with different oxygen octahedral titling modes stabilized by epitaxial strain. Therefore, it is expected to observe the coexistence of different octahedral titling modes with different resultant polarization modulation in the strained ABO_3 thin films. BFO is a very promising porotype[17–20], which has the phase transition that follows the sequence R - M_A(R-like) - M_C (T-like) - T phases[21–24] with the increasing epitaxial strain. The accurately structural determination of BFO has inferred that the T-like phase crystallizes in two different space groups, which correspond to Cc and Cm monoclinic phases that exhibit either an out-of-phase mode (R_4^+) of the oxygen pyramids in two directions or an in-phase mode (M_3^+) in one direction, respectively[25, 26]. Their different oxygen pyramid tilting modes might contribute to the polarization rotation as predicted by first-principles calculations[27].

Here, polarization rotation induced by oxygen pyramid tilting is directly observed by atomic resolution aberration corrected scanning transmission electron microscopy (STEM) in the BFO/$LaAlO_3$(LAO) thin films with an intermediate thickness of 40 nm. Two strain-driven stripe-like supertetragonal phases (monoclinic

Cm and Cc), both with a large tetragonality, exhibit obvious polarization rotation across the phase boundary induced by different oxygen pyramid tilting modes. Moreover, microtwins in the Cc phase with large in-plane polarization are observed, which was not previously observed by X-ray or other macro-structural measurements.

2.! Experimental results and discussion

40 nm and 57 nm BFO thin films were epitaxially grown on (001)-oriented LAO single crystal substrates using pulsed laser deposition (PLD). Figure 1(a) shows a low magnification high-angle annular dark-field STEM (HAADF-STEM) image of a 40 nm BFO film. Stripe-like bright and dark contrast is clearly observed, as shown in the enlarged image in Figure 1(b). It should be noted that the stripe-like contrast can be distinguished from that produced by R-like and T-like phases, which appears in films of greater thickness[20], such as the 57 nm BFO thin film in Figure S1. In order to further understand the atomic structures of the two phases, high-resolution HAADF-STEM images were recorded in Figure 1(d). A Fast Fourier Transform (FFT) is displayed in the inset. The spots in the FFT are split along the c direction because of the large lattice mismatch between LAO and BFO. The c/a ratio is estimated to be ~1.23, as a result of the larger tetragonality of the T-like phase. After carefully examining FFTs from different localized areas, two T-like phases are found in Figure 1(f) and 1(g). The primary difference is the presence of extra !"#$%& superreflection spots. The generation of a digital dark-field (DDF) image from the extra spots base on the STEM images reveals two T-like phases in Figure 1(e).

As the rich phase structures of BFO have already been widely studied before, our results here should be also within the realm of these possibilities. By comparing the two T-like phases with previous experimental and theoretical results and carefully examining these structure models in the literatures[25, 26, 28], it can be inferred that they are monoclinic Cc or Cm phases with the atomic model in Figure 2(a) and 2(d), respectively. Although some other possibilities might exist, the explanations here might be the most reasonable one. More detailed analysis can be found in Figure S2. The phase with the extra !"#$%& spots corresponds to the Cm phase, with an

in-phase mode (M_3^+) of oxygen pyramid tilting in one direction that doubles the unit cell of BFO. Figure 2(b) show the simulated diffraction pattern of Cm phase along the [100] direction, consistent with the FFT analysis above and the nanodiffraction result in Figure 2(c). The oxygen pyramid is ordered along the [110] direction, as indicated by a red dotted line in Figure 2(a), with the oxygen pyramid tilting alternately towards the left or right. Note that the Cm phase here is the same as the T-like phase in the 57 nm BFO film in Figure S1, consistent with previous reports[28, 29]. The phase without the extra ! " #$$%& spots is the Cc phase, which always exists in ultrathin BFO films on LAO[26, 28]. The stripe-like morphology with two T-like phases, rather than a mixture of T-like and R-like phases, is observed at intermediate thicknesses of BFO on LAO. Additionally, the Cc and Cm phases show almost no obvious difference in chemical composition as discussed in Figure S4.

Geometrical phase analysis (GPA)[30] was further used to map the strain fields in the thin films. Figure 3(a) and 3(c) show experimental maps of in-plane (e_{xx}) and out-of-plane (e_{yy}) deformation, respectively. The stripe-like contrast is clear in the in-plane deformation map because of the different in-plane lattice parameters a. However, the deformation e_{xx} is very small, as indicated by the line profile in Figure 3(b). The difference in out-of-plane deformation between the Cm and Cc phases is negligible. Maps of the lattice parameters a, c and c/a determined from accurately measured atomic positions are shown in Figure 3(d-f). These results are consistent with the GPA analysis, with $a_{LAO} ! a_{Cc} > a_{Cm}$ and $c_{Cm} ! c_{Cc} > c_{LAO}$. The large tetragonality of ~ 1.23 and 1.21 are respectively observed for Cm and Cc phases in Figure 3(g), with a transition region of approximately 3–4 unit-cells at both interfaces, indicating a relaxation of the lattice in the growth direction away from the interface[31]. The variation of the in-plane lattice parameter a is shown in Figure 3(h). For the Cc phase, it is uniform throughout the film. While for the Cm phase, it has a constant value only for the first 5-6 unit-cells, after which it gradually decreases by ~5 pm. Therefore, very small difference in lattice parameters and strain are existing between the Cc and Cm phase, except for the different oxygen pyramid tilting modes.

In BFO, the lattice is strongly coupled to the polarization. Different oxygen pyramid tilting modes could lead to different ferroelectric properties of the Cm and Cc phases. Figure 4(a) shows unit cell by unit cell polarization mapping across a phase boundary. The polarization is defined as the displacement of Fe atom columns with respect to the center of four nearest Bi atom columns surrounding it. Figure 4(b) shows a corresponding HAADF-STEM image with an overlaid map of the lattice parameter a, on which the Cm and Cc phases can be identified. The polarization direction rotates from ~87° in the Cm phase to ~64° in the Cc phase, as indicated in Figure 4(c). The Cm phase has a giant out-of-plane and a small in-plane polarization, resulting in a tetragonal-like polarization. In the Cc phase, the in-plane polarization is very high. Though the monoclinic distortions of the Cc phase could explain why the polarization is not aligned strictly along [001] direction[28], it cannot contribute to such a large polarization rotation in the highly tetragonal Cc phase. Apart from the very small difference in lattice parameter a, the different oxygen pyramid tilting modes should be the primary origin of the differently polarized states. The Cc phase with a large in-plane polarization is further confirmed by analyzing different areas in Figure S3 in the stripe-like phases. Note that the tilting angle of the polarization in the Cc phase in Figure S3 does not always have a single value, indicating that there is a different degree of competition in different parts of the film, which might be caused by the varied proportion of microtwins in the Cc phase discussed below. Previous theoretical calculations have revealed the important role of oxygen octahedra tilting, which opposes any natural enhancement of the out-of plane polarization[27]. The antiferrodistortive rotation of oxygen pyramids with an in-phase (R_4^+) mode and polar instabilities of the Cc phase compete with each other and contribute to a ground state that has a large in-plane polarization. The value of polarization remains almost the same for the Cc and Cm phases, as shown in Figure 4(d), in contrast to previous calculations[27] stating that the Cc phase has a lower total amplitude of polarization with a similar misfit when compared with the Cm phase. The c/a value for the Cc phase (~1.21) is much larger than the theoretical prediction (~ 1.15)[27] and not observed before. Our results provide the experimental evidence of a competition

between oxygen pyramid tilting and out-of-plane polarization in the stripe-like morphology of the BFO films.

As the Cc phase with a large in-plane polarization and tetragonality has not been predicted by theoretical calculation, it might be a metastable phase observed here in the strained BFO thin films. The further detailed analysis reveals the microtwins in the Cc phase as shown in Figure 5(a) and 5(b), which are absent in the Cm phase. The microtwins are resolved by giving the rotation angle of atomic planes in the grown direction, which was calculated by the GPA script developed by Christoph T. Koch. We attribute these microtwins to the 180° in-plane rotations in the Cc phase along the [100] or [-100] directions. The corresponding atomic model is shown in Figure 5(c). The rotation angle of ~3.8° in the model is consistent with the experimental rotation map shown in Figure 5(a). The existence of microtwins can partially accommodate the internal strain and stabilize the metastable Cc phase. Obviously, the microtwins are not homogeneous in the Cc phase as shown in Figure 5(a), which might contribute to the varied titling angle of polarization as discussed above.

Based on the above structural and strain analysis of the BFO/LAO thin films, we attribute the formation of these phase structures observed here to the appropriate strain at an intermediate thickness. For very thin BFO film, such as 7 nm as reported before[26], the Cc phase is stabilized in the whole thin films without any microtwins. For the thick BFO film, such as 57 nm here, the Cm and R phases are coexisting. Therefore, the transition from Cc to Cm phase will occur with the increasing film thickness. We speculate the phase evolution as follows. Firstly, the Cc phase is stabilized in the very thin BFO films but the microtwins is absent owing to the fully strain state. Then, with the increasing thickness, partial strain will be gradually relaxed through forming the microtwins in the Cc phase. Furthermore, some regions of Cc phase will transform into the Cm phase with the increasing strain relaxation. Consequently, the stripe-like phase morphology of Cm and Cc phases are formed.

3.! Conclusion

In summary, the nanoscale strain-driven stripe-like supertetragonal phases are observed in a BFO/LAO thin film of intermediate thickness. Stripes are formed of Cc

and Cm phases, with a large tetragonality and different oxygen pyramid tilting modes. The competition between oxygen pyramid tilting and out-of-plane polarization is directly observed, leading to the polarization rotation in the Cc phase. Microtwins in the Cc phase are identified to release the strain of the metastable phase. Our results demonstrate the direct experimental evidence of the interplay between polarization rotation and oxygen pyramid tilting in the strained $BiFeO_3$ thin films, which might be used to design desirable ferroelectric polarization and properties in perovskite oxides.

Acknowledgments

This work was financially supported by Chinese National Natural Science Foundation (51788104, 51390471, 51527803, 51761135131)" National 973 Project of China (2015CB654902), and National key research and development program (2016YFB0700402 and 2016YFA0301001). This work made use of the resources of the National Center for Electron Microscopy in Beijing and the Ernst Ruska-Centre for Microscopy and Spectroscopy with Electrons in Jülich. The research leading to these results received funding from the European Research Council under the European Union's Seventh Framework Programme (FP7/2007-2013)/ ERC grant agreement number 320832. D.S. acknowledges a Scholarship for Overseas Graduate Studies at Tsinghua University.

References

1. Wang KF, Liu J-M, Ren ZF. Multiferroicity: the coupling between magnetic and polarization orders. Advances in Physics. 2009;58(4):321–448.
2. Hwang HY, Iwasa Y, Kawasaki M, Keimer B, Nagaosa N, Tokura Y. Emergent phenomena at oxide interfaces. Nature Materials. 2012;11(2):103–113.
3. Chakhalian J, Freeland JW, Millis AJ, Panagopoulos C, Rondinelli JM. Colloquium: Emergent properties in plane view: Strong correlations at oxide interfaces. Rev Mod Phys. 2014;86(4):1189–1202.
4. Rondinelli JM, Fennie CJ. Octahedral Rotation-Induced Ferroelectricity in Cation Ordered Perovskites. Advanced Materials. 2012;24(15):1961–1968.
5. Kim Y-M, Kumar A, Hatt A, Morozovska AN, Tselev A, Biegalski MD, et al. Interplay of Octahedral Tilts and Polar Order in $BiFeO_3$ Films. Advanced Materials. 2013;25(17):2497–2504.
6. Hatt AJ, Spaldin NA. Structural phases of strained $LaAlO_3$ driven by octahedral tilt instabilities. Phys Rev B. 2010;82(19):195402.
7. Sim H, Cheong SW, Kim BG. Octahedral tilting-induced ferroelectricity in $ASnO_3/BSnO_3$ superlattices. Phys Rev B. 2013;88(1):014101.
8. Borisevich AY, Chang HJ, Huijben M, Oxley MP, Okamoto S, Niranjan MK, et al. Suppression of Octahedral Tilts and Associated Changes in Electronic Properties at Epitaxial Oxide Heterostructure Interfaces. Phys Rev Lett. 2010;105(8):087204.
9. Levin I, Krayzman V, Cibin G, Tucker MG, Eremenko M, Chapman K, et al. Coupling of emergent octahedral rotations to polarization in $(K,Na)NbO_3$ ferroelectrics. Scientific Reports. 2017;7(1):15620.
10. He J, Borisevich A, Kalinin SV, Pennycook SJ, Pantelides ST. Control of Octahedral Tilts and Magnetic Properties of Perovskite Oxide Heterostructures by Substrate Symmetry. Phys Rev Lett. 2010;105(22):227203.
11. Liao Z, Huijben M, Zhong Z, Gauquelin N, Macke S, Green RJ, et al. Controlled lateral anisotropy in correlated manganite heterostructures by interface-engineered oxygen octahedral coupling. Nature Materials. 2016;15(4):425–431.
12. Kan D, Aso R, Sato R, Haruta M, Kurata H, Shimakawa Y. Tuning magnetic anisotropy by interfacially engineering the oxygen coordination environment in a transition metal oxide. Nature Materials. 2016;15(4):432–437.
13. Zhang S, Guo X, Tang Y, Ma D, Zhu Y, Wang Y, et al. Polarization Rotation in Ultrathin Ferroelectrics Tailored by Interfacial Oxygen Octahedral Coupling. ACS Nano. 2018;12(4):3681–3688.
14. Rondinelli JM, Spaldin NA. Substrate coherency driven octahedral rotations in perovskite oxide films. Phys Rev B. 2010;82(11):113402.
15. Benedek N, Rondinelli J, Djani H, Ghosez P, Lightfoot P. Understanding ferroelectricity in layered perovskites: new ideas and insights from theory and experiments. Dalton Transactions. 2015;44(23):10543–10558.
16. Young J, Rondinelli JM. Atomic Scale Design of Polar Perovskite Oxides without Second-Order Jahn–Teller Ions. Chem Mater. 2013;25(22):4545–4550.

17. Catalan G, Scott JF. Physics and Applications of Bismuth Ferrite. Advanced Materials. 2009;21(24):2463–2485.
18. Schlom DG, Chen L-Q, Eom C-B, Rabe KM, Streiffer SK, Triscone J-M. Strain Tuning of Ferroelectric Thin Films. Annual Review of Materials Research. 2007;37(1):589–626.
19. Yang J-C, He Q, Yu P, Chu Y-H. $BiFeO_3$ Thin Films: A Playground for Exploring Electric-Field Control of Multifunctionalities. Annual Review of Materials Research. 2015;45(1):249–275.
20. Zeches RJ, Rossell MD, Zhang JX, Hatt AJ, He Q, Yang CH, et al. A Strain-Driven Morphotropic Phase Boundary in $BiFeO_3$. Science. 2009;326(5955):977.
21. Chen Z, Luo Z, Huang C, Qi Y, Yang P, You L, et al. Low-Symmetry Monoclinic Phases and Polarization Rotation Path Mediated by Epitaxial Strain in Multiferroic $BiFeO_3$ Thin Films. Advanced Functional Materials. 2011;21(1):133–138.
22. Zhang JX, Xiang B, He Q, Seidel J, Zeches RJ, Yu P, et al. Large field-induced strains in a lead-free piezoelectric material. Nature Nanotechnology. 2011;6(2):98–102.
23. Beekman C, Siemons W, Ward TZ, Chi M, Howe J, Biegalski MD, et al. Phase Transitions, Phase Coexistence, and Piezoelectric Switching Behavior in Highly Strained $BiFeO_3$ Films. Advanced Materials. 2013;25(39):5561–5567.
24. Christen HM, Nam JH, Kim HS, Hatt AJ, Spaldin NA. Stress-induced R ! M_A ! M_C ! T symmetry changes in $BiFeO_3$ films. Physical Review B. 2011;83(14).
25. Diéguez O, González-Vázquez OE, Wojde" JC, Íñiguez J. First-principles predictions of low-energy phases of multiferroic $BiFeO_3$. Physical Review B. 2011;83(9).
26. Pailloux F, Couillard M, Fusil S, Bruno F, Saidi W, Garcia V, et al. Atomic structure and microstructures of supertetragonal multiferroic $BiFeO_3$ thin films. Physical Review B. 2014;89(10).
27. Dupé B, Infante IC, Geneste G, Janolin PE, Bibes M, Barthélémy A, et al. Competing phases in $BiFeO_3$ thin films under compressive epitaxial strain. Physical Review B. 2010;81(14).
28. Béa H, Dupé B, Fusil S, Mattana R, Jacquet E, Warot-Fonrose B, et al. Evidence for Room-Temperature Multiferroicity in a Compound with a Giant Axial Ratio. Physical Review Letters. 2009;102(21).
29. Rossell MD, Erni R, Prange MP, Idrobo JC, Luo W, Zeches RJ, et al. Atomic Structure of Highly Strained $BiFeO_3$ Thin Films. Physical Review Letters. 2012;108(4).
30. Hÿtch MJ, Snoeck E, Kilaas R. Quantitative measurement of displacement and strain fields from HREM micrographs. Ultramicroscopy. 1998;74(3):131–146.
31. Huang R, Ding H-C, Liang W-I, Gao Y-C, Tang X-D, He Q, et al. Atomic-Scale Visualization of Polarization Pinning and Relaxation at Coherent $BiFeO_3/LaAlO_3$ Interfaces. Advanced Functional Materials. 2014;24(6):793–799.

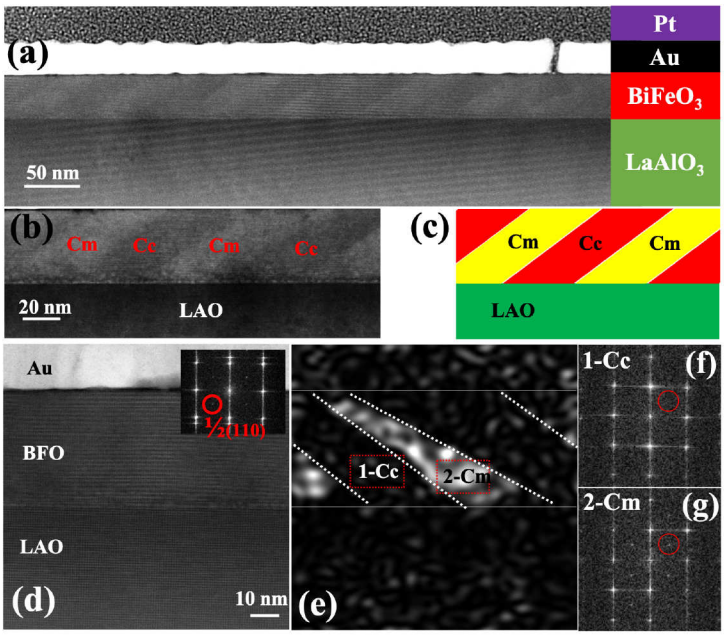

Figure 1 Stripe-like tetragonal phases in BFO/LAO films of thickness 40 nm. (a) Low magnification HAADF-STEM image. (b) Enlarged image and schematic diagram show the stripe-like phases. (d) High-resolution HAADF-STEM image with FFT inset. A red circle marks a $\frac{1}{2}(110)$ extra spot. (e) DDF images generated from the extra spots in (d). (f, g) FFTs of the ***Cc*** and ***Cm*** phases, respectively. All the images are taken under the [100] zone axis.

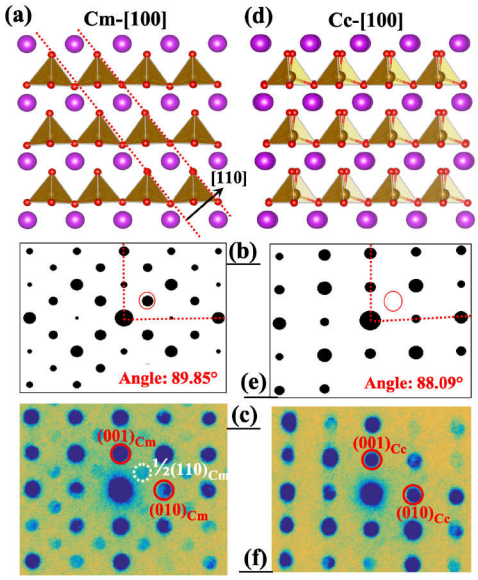

Figure 2 Atomic model and electron diffraction patterns for the *Cm* and *Cc* phases. (a, d) Atomic models of the ***Cm*** and ***Cc*** phases, respectively, viewed along the [100] direction. The red dotted lines mark (110) planes with ordered oxygen pyramid tilting. (b,e) Simulated electron diffraction patterns corresponding to the structural models in (a) and (b) along [100] direction, respectively. (c, f) Electron nanodiffraction patterns of ***Cm*** and ***Cc*** phases, respectively.

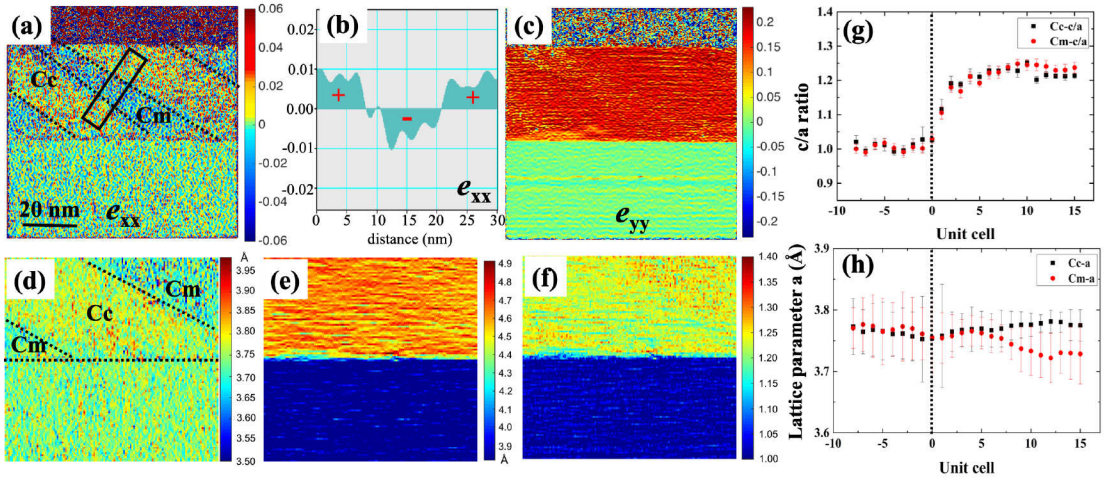

Figure 3 Mapping of strain field and lattice parameters of the stripe-like phases under the [100] zone axis. (a, c) In-plane (e_{xx}) and out-of-plane (e_{yy}) deformation, respectively, measured using GPA. (b) Line profile obtained from the rectangle in (a), illustrating the deformation across the phase boundary. (d-f) Lattice parameters *a*, *c* and *c/a*, respectively. Lattice parameters *c/a* (g) and a (h) of ***Cc*** and ***Cm*** phases measured as a function of distance from the interface in BFO/LAO (40 nm) thin films.

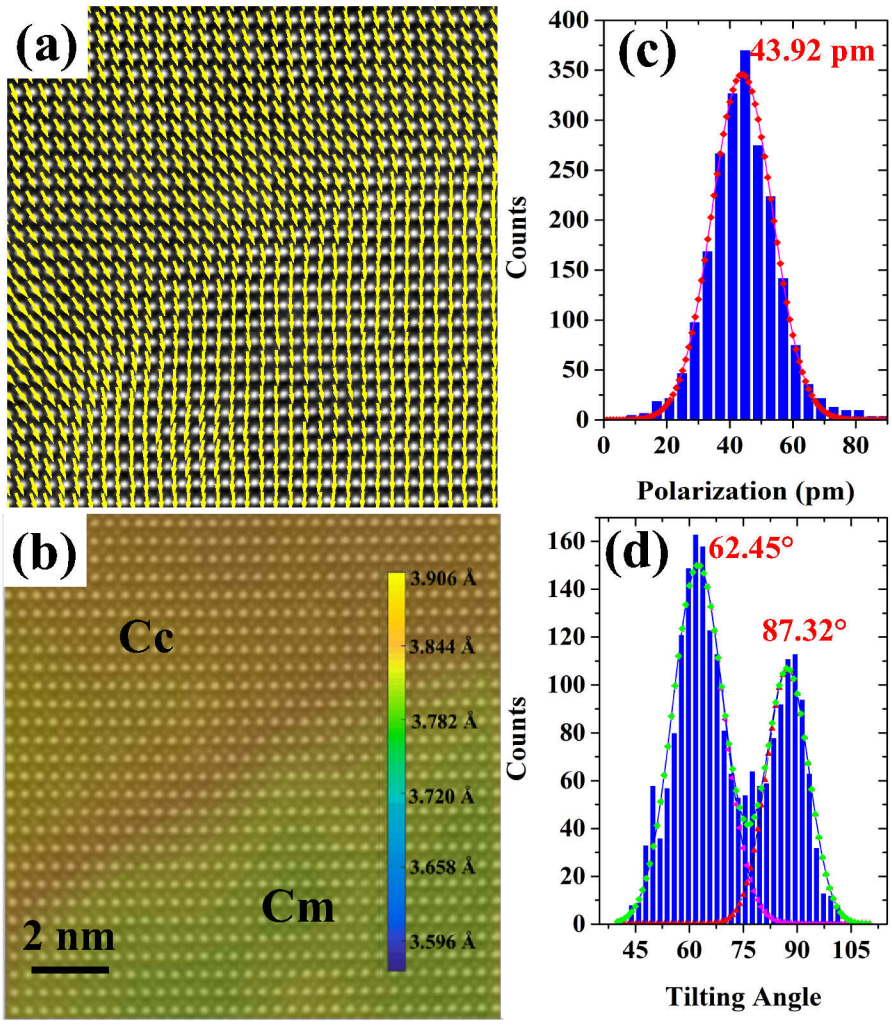

Figure 4 Polarization mapping of the *Cc* and *Cm* phases under [100] zone axis. (a) Mapping of polarization across a phase boundary. (b) Mapping of lattice parameter *a* superimposed onto an HRSTEM image. (c, d) Histograms of polarization and tilt angle from (a), respectively.

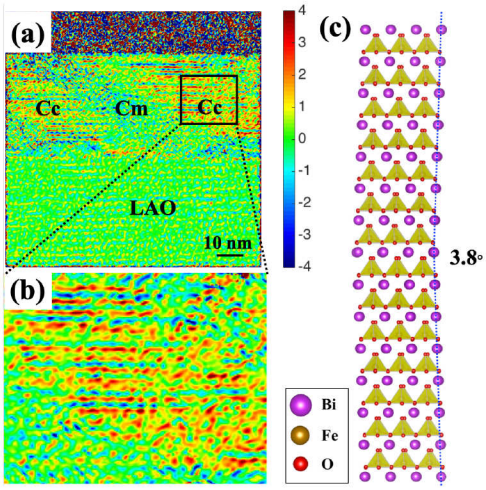

Figure 5 Microtwins in the *Cc* phases under the [100] zone axis. (a) Rotation map of the ***Cc*** and ***Cm*** stripe-like phases in the growth direction. The units in the color bar are degrees. (b) Enlarged area shows microtwins in the ***Cc*** phase in the marked region in (a). (c) Atomic model of an in-plane 180° rotation in the ***Cc*** phase.